

Continuum modeling of shear dilatancy-induced secondary flow in granular media

Gautam Vatsa^{1,*} and Prabhu R Nott^{1,**}

¹Indian Institute of Science, Bangalore, 560012, India

Abstract. This study explores the transient evolution of dilation-driven secondary flows in a dense, slowly sheared granular medium using the non-local continuum model of Dsouza and Nott [1]. In earlier studies, DEM simulations have shown that shear-induced dilatancy, coupled with gravity, sustains a system-spanning secondary vortex in a plane Couette setup with a free surface. We impose a fixed top boundary and a prescribed mean volume fraction to simplify computations. The model captures the emergence of transient, dilation-driven secondary vortices, mirroring qualitative features of the simulations. The magnitude of the secondary velocity is smaller than that in DEM simulations, reflecting suppression of expansion by the fixed boundary. These findings validate the model's robustness and establish a foundation for future studies incorporating free-surface conditions.

1 Introduction

Shear-induced dilatancy, first observed by Osborne Reynolds in 1885 [2], refers to volume change in granular materials when they are subjected to shear deformation. In slow, dense granular flows, this phenomenon leads to complex interactions between the flow kinematics and volume fraction ϕ field ([3, 4]). Most existing continuum models assume incompressibility, neglecting shear dilatancy. The non-local model developed by Dsouza and Nott [1] addresses this limitation and captures shear dilatancy and its coupling with the kinematics. Previous studies have found an excellent agreement with DEM simulations of 1D plane shear [1] and with the data obtained from steady state experiments conducted on a 2D cylindrical Couette rheometer [5].

Krishnaraj and Nott [3] used DEM simulations to show that shearing a column of granular material with a free surface under gravity results in the formation of a system-spanning secondary vortex, driven by the coupling of dilatancy and gravity. Secondary flows have also been explored using hybrid continuum-DEM approaches (e.g., Kim et al., 2023 [6]); resolving such phenomena has remained elusive to purely continuum models. Here, we apply the non-local model of Dsouza and Nott [1] to a plane Couette configuration under gravity, with a fixed top boundary at $z = 0$ that prohibits vertical motion (unlike a free surface, which could displace and deform). We assess its ability to capture the transient evolution of dilation-driven secondary flows, reproduce qualitative features observed in DEM simulations [3], and evaluate the impact of this rigid boundary on their behavior.

2 The non-local model of Dsouza & Nott

The constitutive model used in this study is a non-local extension of the classical critical state plasticity theory proposed by Dsouza and Nott [1]. The central idea behind the model is that the deformation at a given \mathbf{x} in a densely packed granular media does not just depend on the stress $\boldsymbol{\sigma}$ at \mathbf{x} but effectively in the mesoscopic region around \mathbf{x} having a characteristic length scale ℓ . The length scale ℓ characterizes the extent of non-locality in granular media. Similarly, the volume fraction ϕ depends not only on the critical state pressure p_c at \mathbf{x} but on p_c in the mesoscopic volume. The constitutive model relating the stress tensor $\boldsymbol{\sigma}$ to the rate of deformation tensor $\mathbf{D} = (\nabla\mathbf{u} + \nabla\mathbf{u}^T)/2$ in the tensorial form is given as follows:

$$\boldsymbol{\sigma} = -p\boldsymbol{\delta} + \frac{2\mu}{\dot{\gamma}}(p_c\mathbf{D}' - \ell^2\Pi\nabla^2\mathbf{D}') \quad (1a)$$

$$p = p_c\left(1 - \frac{\mu_b}{\dot{\gamma}}\nabla\cdot\mathbf{u}\right) + \ell^2\Pi\frac{\mu_b}{\dot{\gamma}}\nabla^2\nabla\cdot\mathbf{u} \quad (1b)$$

$$p_c = \Pi - \ell^2\frac{d\Pi}{d\phi}\nabla^2\phi \quad (1c)$$

where $\mathbf{D}' \equiv \mathbf{D} - \frac{1}{3}\nabla\mathbf{u}$ is the deviatoric part of \mathbf{D} and $\dot{\gamma} \equiv (2\mathbf{D}' : \mathbf{D}')^{1/2}$ is its scalar invariant, p is the pressure and p_c the pressure at the critical state. The terms multiplied by ℓ^2 are non-local contributions to the constitutive relation. The material properties are the friction coefficients μ and μ_b for shear and volume deformation, respectively, the mesoscopic length ℓ , and the local form of the critical state pressure $\Pi(\phi)$ which is given as follows:

$$\Pi(\phi) = \begin{cases} \alpha \frac{(\phi - \phi_{\min})^{n_1}}{(\phi_{\max} - \phi)^{n_2}}, & \phi \geq \phi_{\min}, \\ 0, & \phi < \phi_{\min} \end{cases} \quad (2)$$

*e-mail: gautamvatsa@iisc.ac.in
 **e-mail: prnott@iisc.ac.in

Here, $\phi_{min} = 0.55$ is the value of loose random packing, and $\phi_{max} = 0.63$ is the value of dense random packing, and α is the stress scale. We retain the form of Π as in [5] by setting $n_1 = 2$ and $n_2 = 1$.

3 Configuration

We consider the flow of granular material in a 2D transient plane shear configuration under gravity, as shown in Figure 1. The flow is assumed to be fully developed in the primary flow direction x . In our setup, the top and bottom boundaries are treated as frictionless rigid plates that allow free slip but are impenetrable. The mean volume fraction of the granular medium is specified, and the change of total volume is restricted at all times, thereby preventing the formation of a free surface.

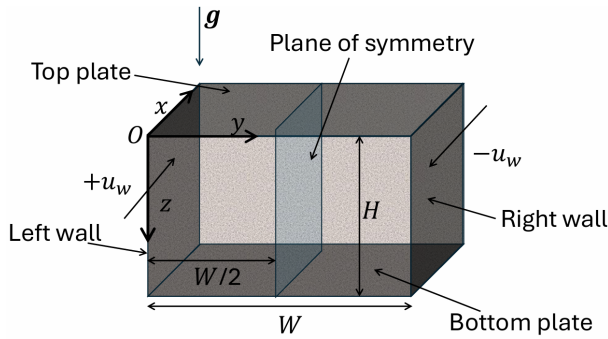


Figure 1. Flow set-up; left frictional wall moves with a velocity $\mathbf{u} = u_w \mathbf{e}_x$; right frictional wall moves with a velocity $\mathbf{u} = -u_w \mathbf{e}_x$; top wall ($y, z = 0$) and bottom wall ($y, z = H$) are stationary frictionless walls; gravity \mathbf{g} is acted along \mathbf{e}_z direction the height of the channel H is $30d_p$, where d_p is the particle diameter and width of the channel W is $30d_p$.

The boundaries at $y = 0$ and $y = W$ are rough, rigid walls that move in opposite directions with velocities $\mathbf{u} = u_w \mathbf{e}_x$ and $\mathbf{u} = -u_w \mathbf{e}_x$, respectively. The top ($z = 0$) and bottom ($z = H$) boundaries are frictionless, while gravity \mathbf{g} acts in the positive z -direction.

4 Governing Equations

The governing equations consist of the mass continuity equation

$$\frac{\partial \phi}{\partial t} + \nabla \cdot (\phi \mathbf{u}) = 0 \quad (3)$$

and Cauchy's momentum balance equations

$$\nabla \cdot \boldsymbol{\sigma} + \rho_p \mathbf{g} \phi = 0 \quad (4)$$

where \mathbf{u} is the velocity vector, $\boldsymbol{\sigma}$ is the stress tensor, ρ_p is the particle density, and \mathbf{g} is the gravitational acceleration. Under the assumptions of slow flow and fully developed profile in x , we discard inertial terms and set $\partial/\partial x = 0$ (see Figure 1) for all field variables. The equations of motion then are

$$\frac{\partial \phi}{\partial t} + \frac{\partial(\phi u_y)}{\partial y} + \frac{\partial(\phi u_z)}{\partial z} = 0 \quad (5a)$$

$$\frac{\partial \sigma_{yx}}{\partial y} + \frac{\partial \sigma_{zx}}{\partial z} = 0 \quad (5b)$$

$$\frac{\partial \sigma_{yy}}{\partial y} + \frac{\partial \sigma_{zy}}{\partial z} = 0 \quad (5c)$$

$$\frac{\partial \sigma_{yz}}{\partial y} + \frac{\partial \sigma_{zz}}{\partial z} = -\rho_p g \phi \quad (5d)$$

The components of the stress tensor $\boldsymbol{\sigma}$ are provided by the non-local model above (Section 2).

4.1 Boundary Conditions

The governing equations (obtained by substituting Equations 1 and 2 in Equation 5) feature fourth-order velocity derivatives and third-order ϕ derivatives, requiring four boundary conditions per velocity component and three for ϕ in y and z directions. These are applied at the shearing walls ($y = 0, z$ and $y = W, z$) and frictionless fixed walls ($y, z = 0$ and $y, z = H$), as shown in Figure 1.

- **Shearing Walls** ($y = 0$ and $y = W$): Tangential velocities follow slip and wall-friction conditions [1, 7]: $\mathbf{n} \cdot \boldsymbol{\sigma} \cdot \mathbf{t} = \mu_w \mathbf{n} \cdot \boldsymbol{\sigma} \cdot \mathbf{n}$ and $\mathbf{u} - \mathbf{u}_w = -K(\mathbf{n} \times \nabla \times \mathbf{u})$, with $\mathbf{u}_w = \pm u_w \mathbf{e}_x$, where \mathbf{t} is the direction of relative velocity between wall and material, and \mathbf{n} is the normal pointing into the medium. The normal velocity is zero. ϕ satisfies $\mathbf{n} \cdot \mathbf{D} \cdot \mathbf{n} / \mathbf{n} \cdot \mathbf{D} \cdot \mathbf{t} = \beta(\phi - \phi_c)$ [5], with critical state value of volume fraction at the boundary ϕ_c prescribed as increasing linearly from 0.565 to 0.595 along z .
- **Frictionless Walls** ($z = 0$ and $z = H$): Tangential velocities obey free-slip, $\mathbf{n} \times \nabla \times \mathbf{u} = 0$ (infinite K), and zero shear stress, $\sigma_{nt} = 0$. Normal velocity is zero. ϕ satisfies $\mathbf{n} \cdot \nabla(\mathbf{n} \cdot \mathbf{D} \cdot \mathbf{n}) = 0$, with $\mathbf{n} \cdot \nabla \phi = 0$ at steady state.
- **General Conditions:** Initial $\phi(\hat{t} = 0, y, z) = 0.6$ is uniform. Steady-state ϕ conditions (prescribed at shearing walls, zero gradient at frictionless walls) are satisfied via coupling with normal velocities and their normal gradients as described above.

The numerical simulations solve a mass continuity equation for a compressible fluid, featuring a time derivative of the volume fraction, coupled with three momentum balance equations. These equations, along with the associated boundary conditions, are discretized using a central finite difference method on a grid of $N_y \times N_z = 51 \times 51$ nodes, yielding a set of coupled nonlinear algebraic equations that are solved via Picard's iteration. Time integration of the mass continuity equation employs an implicit Euler method. The current results are reported for this resolution. We set the values of parameters associated with the shearing walls: the wall friction coefficient $\mu_w = 0.1$, the slip coefficient $K = 1.65$, and the dilation rate proportionality constant $\beta = 1$; and the material parameters: macroscopic friction coefficient $\mu = 1$, bulk viscosity $\mu_b = 0.1$ and the ratio of gravitational stress to the stress scale $\rho_p g d_p / \alpha = 10^{-4}$. Future work involves a more rigorous estimation of these parameters from a comparison with the DEM data.

5 Results and discussion

5.1 Secondary flow during initial stages of shear - small strains

During the initial stages of shear (up to a dimensionless time unit $\hat{t} \sim 5$, where \hat{t} is defined as the product of time t and the nominal shear rate u_w/W), shear dilatancy causes particles to be convected away from the moving walls at $y = 0$ (left) and $y = W$ (right). As established in our prior work [5], the boundary condition dictates that the ratio of the dilation rate normal to the wall to the tangential shear rate is proportional to the departure of the packing fraction, ϕ , from its critical state value at the boundary, defined as $\phi - \phi_c$, where ϕ_c is the critical-state value of ϕ at the wall. We specify that ϕ_c increases linearly in the positive z -direction (aligned with gravity), a simplification reflecting the expected gravitational influence, though its exact variation is uncertain. Initially, ϕ is uniform throughout the system (our initial condition), so the linear increase in ϕ_c with height results in a larger departure ($\phi - \phi_c$) near the top (smaller z), where ϕ_c is greater, and a smaller departure near the bottom ($z = H$).

Consequently, the dilation rate is higher near the top than the bottom, and since a more dilated medium offers less resistance to particle flow, this gradient drives an initial upward motion. However, the medium's inability to expand freely halts this upward flow, redirecting particles downward toward $z = H$ (the system's bottom). In contrast, DEM simulations by [3] show a persistent upward flow, likely due to their free surface, which allows unrestricted expansion, unlike our constrained volume setup.

5.2 Emergence of secondary vortex during intermediate strains

Beyond $\hat{t} \sim 5$, significant gradients in the packing fraction, ϕ , emerge along the z -direction (with $z = 0$ at the top and $z = H$ at the bottom, gravity acting in the positive z -direction). These gradients halt the downward particle motion toward $z = H$, causing streamlines to curve upward toward $z = 0$, against gravity, and initiate vortex-like flow. During this intermediate stage, the emerging vortex resembles the flow patterns observed in the initial shear stages of the DEM simulations by [3]. By $\hat{t} \sim 9$, two system-spanning, counter-rotating vortices form, centered near the top-left ($y = 0, z = 0$) and top-right ($y = W, z = 0$) corners, as depicted in Figure 2. At larger strains ($\hat{t} > 10$), these secondary vortices elongate along the z -direction, closely resembling the steady-state vortex structures in Krishnaraj and Nott (2016). However, numerical inaccuracies at very large strain ($\hat{t} > 13$) prevent us from confirming sustained vortex flow. Nevertheless, as shown in Figure 3, the mean magnitude of secondary velocities (perpendicular to the shear direction), normalized by wall velocities, saturates at a non-zero value, suggesting a likely persistent steady-state vortex. This magnitude is substantially smaller than that in DEM simulations of [3], indicating that the fixed boundary in our system—or the absence of a free surface—strongly suppresses secondary flow.

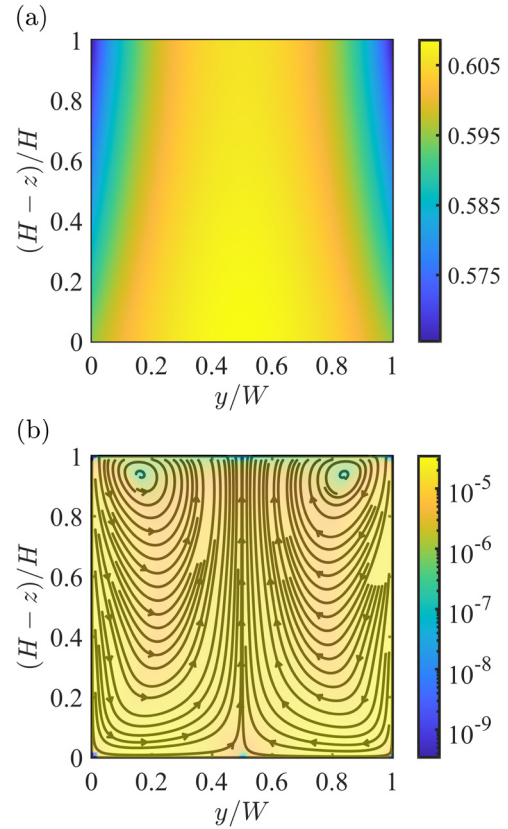


Figure 2. Emergence of secondary vortex flow at intermediate dimensionless time \hat{t} ; (a) shows the density ϕ map at $\hat{t} = 9$ where the colorbar indicate ϕ and (b) shows secondary flow streamlines at $\hat{t} = 9$ - the colorbar indicate the magnitude of secondary velocity scaled by the wall velocity $\frac{\sqrt{u_y^2 + u_z^2}}{u_w}$

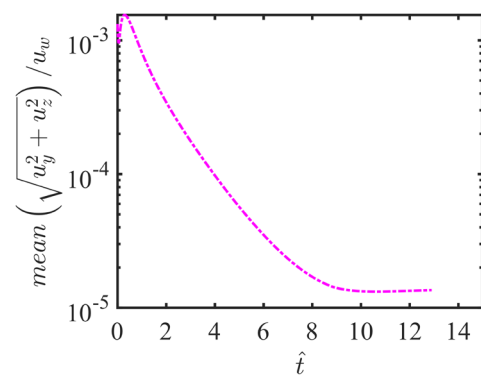


Figure 3. Time evolution of the mean over all spatial locations of magnitude of velocity in the secondary plane $\sqrt{u_y^2 + u_z^2}$ scaled by the wall velocity u_w

5.3 Coupling between dilatancy and primary velocity

So far, we have shown how dilatancy drives secondary flow and how its transient evolution is closely linked to the evolution of ϕ . However, the non-local model also predicts

a strong coupling between the primary velocity field u_x and ϕ . In conjunction with our earlier findings [5], the model predicts that as the material dilates near the shearing walls, there is an enhanced slip, as shown in Figure 4.

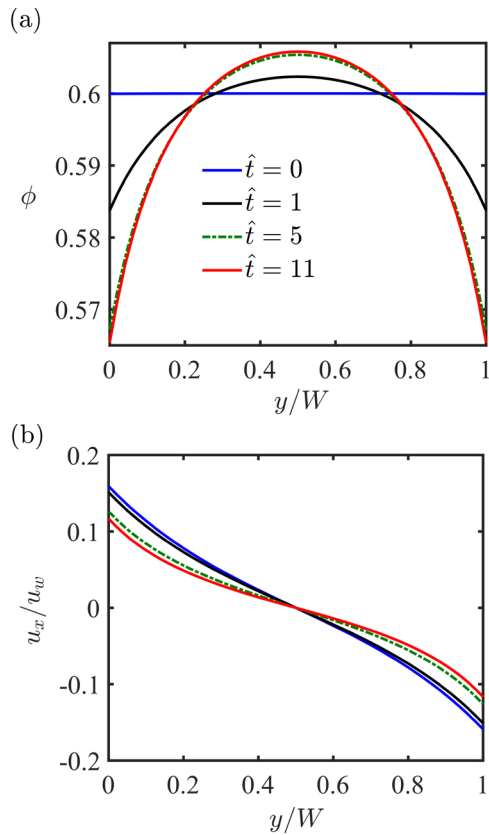


Figure 4. Time evolution of (a) ϕ at the top boundary ($z = 0$) and (b) primary velocity u_x scaled by the wall velocity u_w at the top boundary ($z = 0$)

6 Conclusion

The non-local continuum model of [1] effectively captures the transient emergence of dilation-driven secondary flows in a sheared granular medium, qualitatively aligning with

features observed in DEM simulations. To our knowledge, only one prior study [6] models secondary flow in an inclined chute using a second-order continuum approach. However, that study falls short of full continuum modeling due to two critical limitations: it bypasses the mass continuity equation by extracting the entire ϕ field directly from DEM data, and it incorporates a free surface by coupling finite difference simulations with DEM inputs. In contrast, this work represents, to our knowledge, the first fully continuum simulation of dilatancy-driven secondary flow, resolving all kinematic fields and the evolution of volume fraction in slow granular flow without DEM-derived inputs. Despite employing simplified boundary conditions and lacking a free surface, our model successfully reproduces vortex formation. In future work we will replace the rigid boundary at the top with a free surface, so that a better comparison with DEM simulations and experiments can be made.

References

- [1] P.V. Dsouza, P.R. Nott, A non-local constitutive model for slow granular flow that incorporates dilatancy, *Journal of Fluid Mechanics* **888**, R3 (2020).
- [2] O. Reynolds, Lvii. on the dilatancy of media composed of rigid particles in contact. with experimental illustrations, *The London, Edinburgh, and Dublin Philosophical Magazine and Journal of Science* **20**, 469 (1885).
- [3] K. Krishnaraj, P.R. Nott, A dilation-driven vortex flow in sheared granular materials explains a rheometric anomaly, *Nature communications* **7**, 10630 (2016).
- [4] P.V. Dsouza, P.R. Nott, Dilatancy-driven secondary flows in dense granular materials, *Journal of Fluid Mechanics* **914**, A36 (2021).
- [5] G. Vatsa, F. Fazelpour, R. Gautam, K.E. Daniels, P.R. Nott, Dilatancy and its coupling to the kinematics in sheared granular media, *Journal of Fluid Mechanics* **1003**, A11 (2025).
- [6] S. Kim, K. Kamrin, A second-order non-local model for granular flows, *Frontiers in Physics* **11**, 1092233 (2023).
- [7] K.K. Rao, P.R. Nott, *An Introduction to Granular Flow* (Cambridge University Press, New York, 2008)